

Effect of cations on the structure of sodium bis(2-ethylhexyl)sulfosuccinate water-in-oil microemulsion

Rika Kawai-Hirai^a and Mitsuhiro Hirai^{b*}^aMeiwa Gakuen Junior College, Maebashi, Gunma 371-0034, Japan, and ^bDepartment of Physics, Gunma University, Maebashi 371-8510, Japan. Correspondence e-mail: mhirai@fs.aramaki.gunma-u.ac.jp

We have characterized the structure of water/sodium bis(2-ethylhexyl)sulfosuccinate (AOT)/isooctane water-in-oil microemulsion depending on the concentrations of monovalent and divalent cations (Na^+ , K^+ , Ca^{2+}) in the water pool. We have found that the presence of salts affects the microemulsion structures differently at low and high water contents. Increasing the salt concentration suppresses the oligomerization of the microemulsions at low water content, whereas it reduces the microemulsion radius at high water content. The present results clearly indicate that not only electrostatic repulsion between AOT headgroups but also negative or positive hydration effects by salts dominate the structure and dynamics of AOT microemulsions, as suggested by a recent molecular dynamics simulation.

© 2007 International Union of Crystallography
Printed in Singapore – all rights reserved

1. Introduction

As we reported previously, the AOT water-in-oil (w/o) microemulsion system forms three different structural phases (oligomeric phase, transient phase and monomeric phase) with increasing w_0 values ($w_0 = [\text{water}]/[\text{AOT}]$) (Hirai, Kawai-Hirai, Yabuki *et al.*, 1995; Hirai, Kawai-Hirai, Takizawa *et al.*, 1995). The transient phase region depends on the linear hydrocarbon chain length of apolar solvent and there exists a penetration limit of apolar solvent into the AOT surfactant (Hirai, Kawai-Hirai, Sanada *et al.*, 1999). In the present report, we show how cations in the water pool affect the AOT w/o microemulsion structures, since cations are expected to change both the microenvironment of the AOT hydrophilic head portion and the water structure (Leodidis & Hatton, 1989). Water-soluble enzymes entrapped in w/o microemulsions are known to show much higher catalytic activity compared to those in appropriate aqueous solvents, which has attracted significant interest for possible practical applications such as microreactors (Pileni, 1989). In fact, the hydrolysis of esters catalysed by α -chymotrypsins or bovine serum albumin entrapped in AOT w/o microemulsions is greatly enhanced at low water content around $w_0 \simeq 12$ (Hirai, Kawai-Hirai, Takizaki *et al.*, 1995; Kawai-Hirai *et al.*, 1995). We also showed that the proteins are occluded in the water pools of the microemulsion with minor changes both in the microemulsion structure and in the protein secondary structure (Kawai-Hirai & Hirai, 2003). Our previous results indicate that the presence of the oligomeric phase of the w/o microemulsion in this low w_0 range is essential for the enhancement of catalytic activity of the enzymes entrapped in w/o microemulsions for use as microreactors for process-engineering applications. The importance of the interfacial properties and droplet size on enzyme activity have also been suggested (Freeman *et al.*, 2000; El-Batal *et al.*, 2005).

The presence of salts in the water pools of w/o microemulsions has been assumed to affect the microemulsion structures (Leodidis & Hatton, 1989). Recently, theoretical studies on the structure of reversed micelles (w/o microemulsion at low water content) occluding small amounts of water and ions have been carried out

(Faeder & Ladanyi, 2000; Bulavchenko *et al.*, 2002; Abel *et al.*, 2004; Pal *et al.*, 2005). Experimentally, the effect of salts on the AOT w/o microemulsion have been studied intensively by using various spectroscopic methods such as infrared, dielectric, conductivity, luminescence, electron paramagnetic resonance and nuclear magnetic resonance (Eastoe *et al.*, 1992; Fioretto *et al.*, 1999; Alvarez *et al.*, 1999; Pitzalis *et al.*, 2000; Burrows & Tapia, 2002). In spite of these previous studies, there is little direct evidence about the effect of different salts on the microemulsion structures (Capuzzi, 1997). Therefore, by using the small-angle X-ray scattering (SAXS) technique we have studied the effect of cations (Na^+ , K^+ , Ca^{2+}) on the structure of the water/AOT/isooctane system.

2. Materials and method

2.1. Materials

AOT was purchased from Nacalai Tesque Inc. 99+% isooctane, sodium chloride, potassium chloride and calcium chloride were purchased from Wako Pure Chemical Industries Ltd. Water purified by a Millipore system was used. The w/o samples were obtained by using an injection method. The water content in the reversed micellar solutions were determined by the Karl Fischer method using a Metrohm 684 KF coulometer. The water-to-surfactant molar ratio w_0 was varied from 0 to 50. The AOT molar concentrations were 0.1 and 0.05 M. The sodium and potassium salt concentrations were varied from 10 to 100 mM. The calcium salt concentration was varied from 2 to 50 mM.

2.2. X-ray scattering measurements and data analysis

SAXS experiments were carried out by using a SAXS instrument installed at the synchrotron radiation source (PF) at the High Energy Accelerator Research Organization (KEK), Tsukuba, Japan (Ueki *et al.*, 1985). A one-dimensional position-sensitive proportional counter detected the scattering intensities. Sample solutions were contained in mica-window cells with 1 mm path length, which were placed in a

cell holder kept at 298 K. The X-ray wavelength used was 1.49 Å. The exposure time was 300 s for each sample.

The details of the SAXS data analyses have been described elsewhere (Hirai, Kawai-Hirai, Yabuki *et al.*, 1995; Hirai, Kawai-Hirai, Takizawa *et al.*, 1995). The following standard analyses were carried out. The distance distribution function $p(r)$ was obtained by Fourier transformation of the observed scattering intensity $I(q)$ as

$$p(r) = (1/2\pi^2) \int_0^\infty rqI(q) \sin(rq) dq, \quad (1)$$

where $q = (4\pi/\lambda)\sin(\theta/2)$, θ is the scattering angle and λ is the X-ray wavelength. The radius of gyration R_g was determined by

$$R_g^2 = \frac{\int_0^{D_{\max}} p(r)r^2 dr}{2 \int_0^{D_{\max}} p(r) dr}, \quad (2)$$

where D_{\max} is the maximum diameter of the particle estimated from the $p(r)$ function satisfying the condition $p(r) = 0$ for $r > D_{\max}$. The Guinier approximation for estimating R_g occasionally leads to inherent systematic errors caused by an interparticle interaction between solute particles (Hirai *et al.*, 1988). Equation (2) can be used to reduce such artifacts for the R_g estimation (Feigin & Svergun, 1987; Hirai, Iwase & Hayakawa, 1999).

3. Results

Fig. 1 (a), (b), (c) and (d) show the w_0 dependence of the SAXS curves of 0.1 M AOT w/o microemulsions at 298 K, where (a), (b), (c) and (d) correspond to 50 mM KCl, 50 mM NaCl, 10 mM CaCl₂ and without salts, respectively. Fig. 1 is plotted on both logarithmic scales. The w_0 value is varied from 0 to 50. As the w_0 value changes from 0 to 50, the scattering intensity in the small- q region increases significantly accompanying the shift of the shoulder of the SAXS curve from ~ 0.15 to ~ 0.03 Å⁻¹, which results from the enlargement of the microemulsion structure due to the occlusion of water in the water pool.

Fig. 2 shows the distance distribution functions, $p(r)$, obtained from the Fourier transformation using equation (1) of the SAXS data in Fig. 1, where (a), (b), (c) and (d) are as in Fig. 1. In Fig. 2 the $p(r)$ functions at $0 < w_0 \leq 8$ clearly have a peak in the short distance region followed by a tail or a shoulder in the long distance region, whereas the $p(r)$ functions at other w_0 values mostly show symmetric bell-shaped profiles. The bell-shaped profiles are attributable to the globular structure of the microemulsions. As shown previously (Hirai, Kawai-Hirai, Yabuki *et al.*, 1995; Hirai, Kawai-Hirai, Takizawa *et al.*, 1995; Hirai, Kawai-Hirai, Sanada *et al.*, 1999), this results from the presence of the oligomeric phase at low water content in the range $0 < w_0 \leq 8$, which is also supported by the following analyses. Figs. 3 and 4 show the w_0 dependence of the radius of gyration, R_g obtained from equation (2), and of the peak position of the $p(r)$ function in Fig. 2, PR_{\max} , where (a), (b) and (c) correspond to the AOT w/o microemulsions whose water pools contain 0–100 mM KCl, 0–100 mM NaCl and 0–50 mM CaCl₂, respectively. As an observed R_g value for a polydisperse system is known to be given by the z -averaged R_g of all solute particles (Hirai *et al.*, 1988), R_g is very sensitive to the presence of oligomeric particles. On the other hand, the PR_{\max} value corresponds well to the radius of the spherical particles in the case of a solution system composed of identical particles.

In Fig. 3 the relation between R_g and w_0 for the microemulsion without salts is characterized by three different regions. At low water content ($0 < w_0 \leq 8$) R_g increases significantly with w_0 . This increase stops at $8 \leq w_0 \leq 16$, and at $w_0 > 16$ R_g begins to increase again linearly with w_0 .

On the other hand, in Fig. 4 for the case without salts the linear relation between PR_{\max} and w_0 holds for the entire range of w_0 . Such relations of R_g versus w_0 and of PR_{\max} versus w_0 are generally observed for all AOT w/o microemulsions composed of different apolar solvents and AOT concentrations (Hirai, Kawai-Hirai, Sanada *et al.*, 1999). The slope of 1.44 ± 0.01 for the microemulsion without salts in Fig. 4 is described principally by the following simple relation between the water pool radius (core radius) r_w and the water content w_0 :

$$r_w = (3v_w/\Sigma)w_0. \quad (3)$$

This equation is well known for w/o microemulsions (Pileni, 1989) and can be derived from geometric consideration of the dimension and packing of surfactant molecules (Israelachvili *et al.*, 1976; Mitchell & Ninham, 1981). In equation (3), v_w and Σ are the volume of a water molecule and the area per polar head of the surfactant molecule, respectively. ($v_w = \sim 30$ Å³ and $\Sigma = \sim 60$ Å² for AOT gives a slope of ~ 1.5 .) The slope in Fig. 4 depends slightly on the hydrocarbon chain length of the apolar solvent due to the penetration of the solvent molecule into the hydrophobic tail region of the surfactant (Hirai, Kawai-Hirai, Sanada *et al.*, 1999). The intercept value obtained from the linear least-squares fitting in Fig. 4, which corresponds to the microemulsion radius at $w_0 = 0$, is 16.2 ± 0.3 Å. This value agree well with that reported by other authors (Kotlarchyk *et al.*, 1985). In addition, the slope of ~ 1.2 at $w_0 \geq 16$ for the microemulsion without salts in the relation of R_g versus w_0 in Fig. 3 is also reasonably explained by equation (3) when we take into account the scattering density distribution the microemulsion. The slope of 2.2 ± 0.2 at $0 < w_0 \leq 8$ in Fig. 3 is much steeper than 1.2, which is followed by the flat region at $8 \leq w_0 \leq 16$. Combined with the tailing profiles in Fig. 2 these deviations from the simple relation of equation (3) in Fig. 3 clearly indicate the presence of oligomeric particles with an identical radius in the solutions at low water content $w_0 \leq 16$ (Hirai, Kawai-Hirai, Yabuki *et al.*, 1995; Hirai, Kawai-Hirai, Takizawa *et al.*, 1995). We previously called these different regions of $0 < w_0 \leq 8$, $8 \leq w_0 \leq 16$ and $w_0 \geq 16$ the oligomeric phase, transient phase and monomeric phase, respectively.

From Figs. 3 and 4 we can understand the following tendencies about the effect of the presence of salts within the water pool on the microemulsion structure. The oligomeric and transient phase regions become narrower or shallower with increasing salt concentration. This tendency is clearer for K⁺ in comparison with the cases of Na⁺ and Ca²⁺. Namely, the slope at $0 < w_0 \leq 8$ decreases from 1.69 ± 0.2 to 1.27 ± 0.08 for K⁺ and from 2.3 ± 0.3 to 1.9 ± 0.3 for Na⁺. In the case of Ca²⁺ the slope varies from 2.27 ± 0.09 to 1.82 ± 0.15 . The approach of the slope at $0 < w_0 \leq 8$ to 1.2 suggests a decrease in the oligomeric particles. This change occurs more clearly for K⁺. In the monomeric phase region ($w_0 \geq 20$), the relation of R_g versus w_0 has a kink at high water content and greatly deviates from the linear relation shown for the microemulsion without salts.

On the other hand, as shown in Fig. 4, at low water content ($w_0 \leq 20$) the linear relation between PR_{\max} and w_0 holds well for the microemulsions in spite of the change of the salt concentration. The slopes are 1.40 ± 0.03 for K⁺ at 10 mM, 1.39 ± 0.03 for K⁺ at 100 mM, 1.36 ± 0.02 for Na⁺ at all concentrations, 1.38 ± 0.02 for Ca²⁺ at 2 mM and 1.34 ± 0.02 for Ca²⁺ at 50 mM. The average intercept values of PR_{\max} ($w_0 = 0$) are 16.4 ± 0.3 Å for K⁺, 16.5 ± 0.2 Å for Na⁺ and 16.6 ± 0.3 Å for Ca²⁺. Although the slopes at $w_0 \leq 20$ show weak dependence on the species and concentration of the salts, the intercept values agree within experimental errors for all salts because these values are essentially determined by an icosahedral packing of AOT polar heads at $w_0 = 0$ (Kotlarchyk *et al.*, 1985). Alternatively, the

above values indicate that the present results are reasonable. At $w_0 \geq 20$ the slope gradually deviates from the initial one with increasing salt concentration. The water content at which deviation from the initial slope of 1.44 starts depends on both the species and concentration of the salts. In the case of K^+ the water contents are $w_0 \approx 30$ –40 for 10 and 20 mM, $w_0 \approx 25$ –30 for 50 mM, and $w_0 \approx 20$ –25 for 100 mM. In the case of Na^+ , $w_0 \approx 30$ –40 for 10, 20 and 50 mM, and $w_0 \approx 25$ –30 for 100 mM. In the case of Ca^{2+} , $w_0 \approx 30$ –50 for 2, 10 and 25 mM, and $w_0 \approx 20$ –25 for 50 mM.

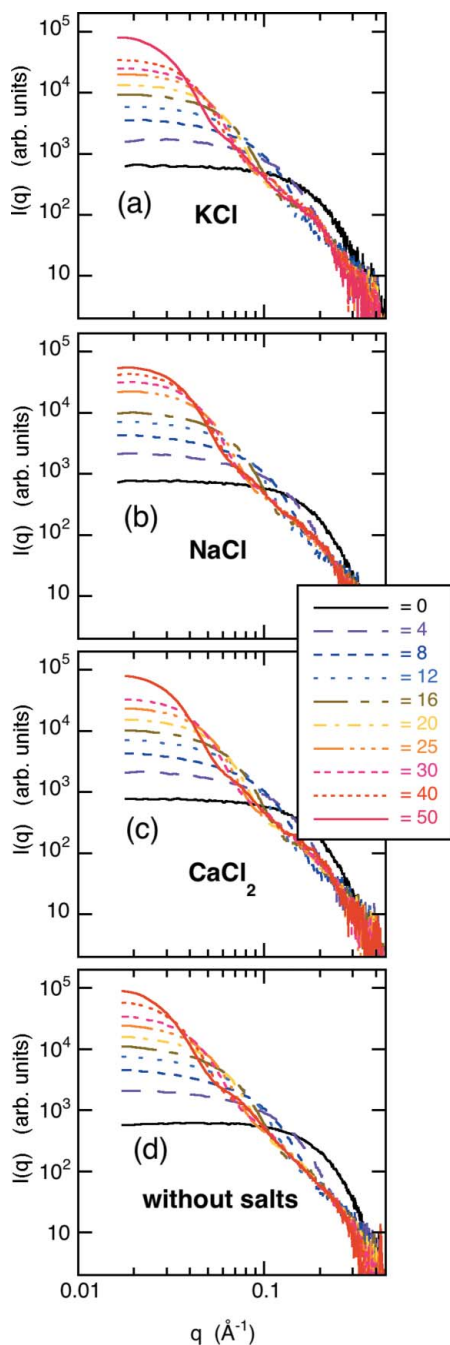


Figure 1
SAXS curves of 0.1 M water/AOT/isoctane w/o microemulsions at 298 K depending on water content and on salt species, where (a), (b), (c) and (d) correspond to 50 mM KCl, 50 mM NaCl, 10 mM $CaCl_2$, and without salts, respectively. The values of w_0 ($= [water]/[AOT]$) are shown in the figure.

Fig. 5 summarizes the salt concentration dependence of the PR_{max} values at different w_0 values, where (a), (b) and (c) are as in Fig. 3. At low water content ($w_0 \leq 20$) the effect of the presence of salts on the structure is relatively small for all cases of the microemulsions with different salts. However, on increasing the water content from $w_0 = 20$ to 50 the presence of salts in the water pool reduces the droplet radius more clearly. In the cases of the monovalent cations, the decrease of the radius for K^+ is larger than that for Na^+ . The divalent cation, Ca^{2+} , reduces the radius more significantly than the monovalent cations.

4. Discussion

The present results are summarized as follows. In the case of AOT w/o microemulsions the slope of R_g at low water content suggests that the appearance of the oligomeric droplets at $w_0 \leq 8$ is suppressed by the increase in salt concentration. Such suppression occurs most clearly for K^+ . The change of R_g also indicates a decrease of the transient phase region ($8 \leq w_0 \leq 16$), which depends on the cation species and concentration. In spite of the decrease of the oligomeric particles, the w_0 dependence shows the linear relation between the water content and the droplet radius in this w_0 range. At high water content (in the

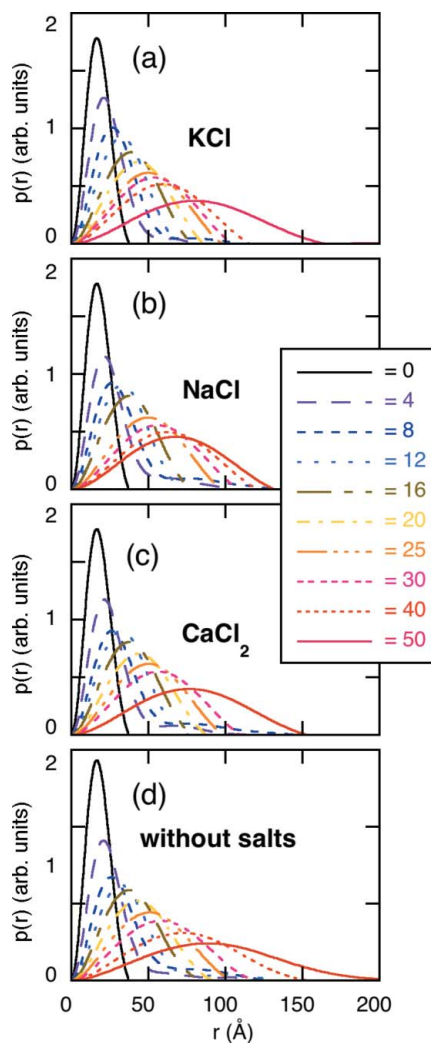


Figure 2
Distance distribution functions, $p(r)$, obtained from the Fourier transformation using equation (1) of the SAXS data in Fig. 1, where (a), (b), (c) and (d) are as in Fig. 1.

monomeric phase, $w_0 \geq 20$) the relation between PR_{\max} and w_0 deviates from this slope and the droplet radius decreases with increasing salt concentration. The deviation is most evident for Ca^{2+} . According to our previous results (Hirai, Kawai-Hirai, Yabuki *et al.*, 1995), below an AOT concentration of 0.1 M any excluded volume effect among the droplets at high water content can be ignored since the linear relation between w_0 and PR_{\max} holds well, which is also clearly seen in Fig. 4. In general, the droplet radius of the w/o microemulsion depends on the water pool radius given in equation (3). In equation (3), the Σ value is given by (Israelachvili, 1992)

$$\Sigma = e(D/2\epsilon\gamma)^{1/2}, \quad (4)$$

where γ is the oil–water surface tension, e is the charge per surfactant molecule, D is the thickness of the diffuse electric double layer and ϵ is the local dielectric constant. Although the exact values of γ and ϵ are unknown, we can estimate the relative change of D depending on the salt concentration. For example, the ratio of $D_{100\text{ mM}}/D_{20\text{ mM}}$ for NaCl is 9.61/21.5, and the ratio of $D_{50\text{ mM}}/D_{10\text{ mM}}$ for CaCl_2 is 7.87/17.6 (Israelachvili, 1992). Experimentally the change of PR_{\max} in Fig. 4 is from 80 to 58 Å for NaCl from 20 mM to 100 mM at $w_0 = 50$, and from

77 to 50 Å for CaCl_2 from 10 mM to 50 mM at $w_0 = 50$. Based on the simple assumption given by equation (4) and on the definition of the electric double layer, the change of PR_{\max} can be calculated to be from 80 to 53 Å for NaCl and from 77 to 52 Å for CaCl_2 . As the estimated values agree qualitatively with the experimental ones, the reduction of the droplet radius at high water content is attributable to the change of Σ . Alternatively, at high water content the presence of salts in water pool would not only affect the electrostatic repulsion between the polar heads of the surfactants, but would also dominate the surface area of the surfactant and the droplet radius as in the bulk solvent due to the enlargement of the water pool radius.

On the other hand, at low water content, $w_0 \leq 20$, the linear relation between the droplet radius and w_0 suggests that the droplet radius is dominated by the width of the Stern layer, not by the diffuse double layer. The suppression of the appearance of the oligomeric phase at low water content induced by the increase in salt concentration can be explained by the reduction of the dynamic fluctuation of the microemulsion that is assumed to play an essential role in the appearance of the oligomeric phase (Hirai, Kawai-Hirai, Iwase *et al.*, 1999). The above interpretation is supported by other evidence. A recent theoretical study using Monte Carlo and molecular dynamics

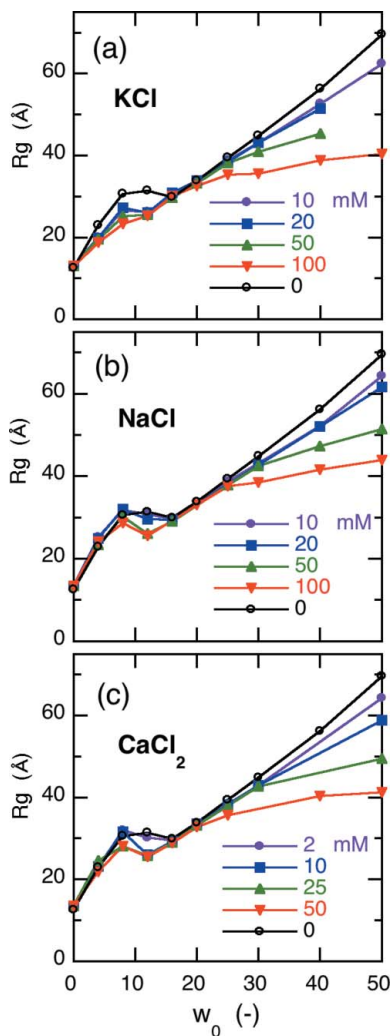


Figure 3 Radius of gyration of water/AOT/isoctane microemulsions depending on w_0 value and on salt concentration, where (a), (b) and (c) correspond to KCl, NaCl and CaCl_2 , respectively. The salt concentrations in the water pools were changed from 0 to 100 mM for KCl, from 0 to 100 mM for NaCl and from 0 to 50 mM for CaCl_2 .

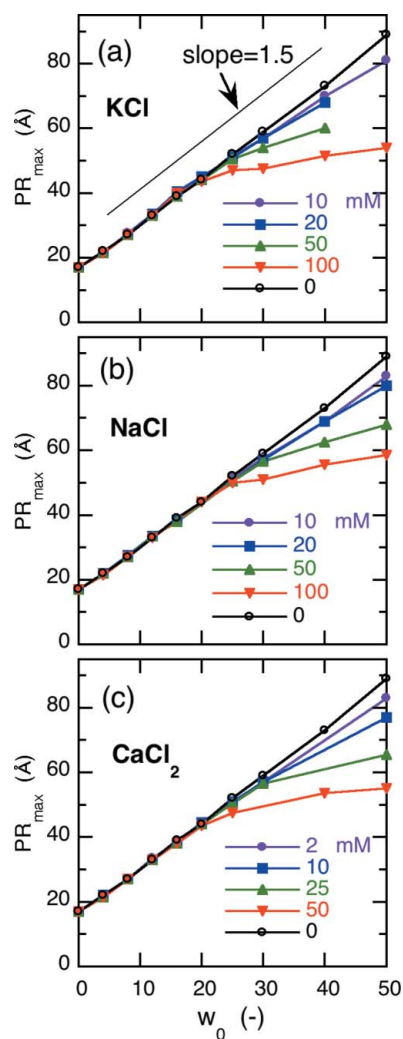


Figure 4 Water-content dependence of the peak position PR_{\max} of the $p(r)$ functions, where (a), (b) and (c) are as in Fig. 3. The salt concentrations in the water pools were changed as in Fig. 3.

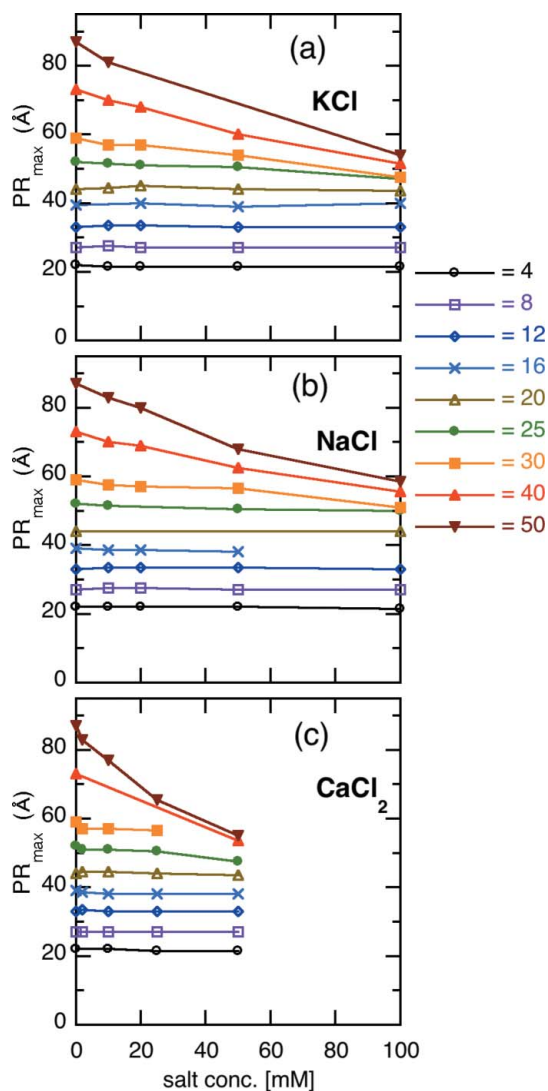


Figure 5
Salt concentration dependence of PR_{max} values at different w_0 values, where (a), (b) and (c) are as in Fig. 3.

simulations has shown two different ion-exchange processes around the headgroups in the AOT reversed micelle ($w_0 \leq 4$) which depend on the species of alkali-metal salts (Pal *et al.*, 2005), indicating that the larger K^+ ions are preferentially localized around the headgroup region due to the difference in solvation energies of different ions. In addition, the boundary between positive and negative hydrations is in between Na^+ and K^+ ions, and K^+ ions work as water-structure breakers (Mazitov, 1981; Uedaira & Tataru, 1998). Thus, the present result on the narrowing of the oligomeric and transient phase regions seen clearly for K^+ at low water content would be attributable to the characteristics of K^+ ions that change the dynamics of the surface area of the droplet. The present results support a recent molecular dynamics simulation result (Chen *et al.*, 2006).

The SAXS experiments were done under the approval of the Photon Factory Program Advisory Committee of KEK (Proposal No. 2002G162).

References

Abel, S., Sterpone, F., Bandyopadhyay, S. & Marchi, M. (2004). *J. Phys. Chem. B*, **108**, 19458–19466.

Alvarez, E., Garcia-Rio, L., Mejuto, J. C., Navaza, J. M. & Perez-Juste, J. (1999). *J. Chem. Eng. Data*, **44**, 850–853.

Bulavchenko, A. I., Batishchev, A. F., Batishchev, E. K. & Torgov, V. G. T. (2002). *J. Phys. Chem.* **106**, 6381–6389.

Burrows, H. D. & Tapia, M. J. (2002). *Langmuir*, **18**, 6706–6708.

Capuzzi, G., Pini, F., Gambi, C. M. C., Monduzzi, M., Baglioni, P. & Teixeira, J. (1997). *Langmuir*, **13**, 6927–6930.

Chen, Y. J., Xu, G. Y., Yuan, S. L. & Sun, H. Y. (2006). *Colloid. Surf. A*, **273**, 174–178.

Eastoe, J., Fragneto, G., Robinson, B. H., Towey, T. T., Heenan, R. K. & Leng, F. J. (1992). *J. Chem. Soc. Faraday Trans.* **88**, 461–471.

El-Batal, A. I., Atia, K. S. & Eid, M. (2005). *Radiat. Phys. Chem.* **74**, 96–101.

Faeder, J. & Ladanyi, B. M. (2000). *J. Phys. Chem.* **104**, 1033–1046.

Feigin, L. A. & Svergun, D. I. (1987). *Structure Analysis by Small-Angle X-ray and Neutron Scattering*. New York: Plenum Press.

Fioretto, D., Freda, M., Mannaioli, S., Onori, G. & Santucci, A. (1999). *J. Phys. Chem. B*, **103**, 2631–2635.

Freeman, K. S., Tang, T. T., Shah, D. E., Kiserow, D. J. & McGown, L. B. (2000). *J. Phys. Chem. B*, **104**, 9312–9316.

Hiragi, Y., Inoue, H., Sano, Y., Kajiwara, K., Ueki, T., Kataoka, M., Tagawa, H., Izumi, Y., Muroga, Y. & Amemiya, Y. (1988). *J. Mol. Biol.* **204**, 129–140.

Hirai, M., Iwase, H. & Hayakawa, T. (1999). *J. Phys. Chem. B*, **103**, 10136–10142.

Hirai, M., Kawai-Hirai, R., Iwase, H., Mitsuya, S., Takeda, T. & Seto, H. (1999). *J. Phys. Chem. Solids*, **60**, 1359–1361.

Hirai, M., Kawai-Hirai, R., Sanada, M., Iwase, H. & Mitsuya, S. (1999). *J. Phys. Chem. B*, **103**, 9658–9662.

Hirai, M., Kawai-Hirai, R., Takizawa, T., Yabuki, S., Oya, M., Nakamura, K., Kobayashi, K. & Amemiya, Y. (1995). *J. Chem. Soc. Faraday Trans.* **91**, 1081–1089.

Hirai, M., Kawai-Hirai, R., Yabuki, S., Takizawa, T., Hirai, T., Kobayashi, K., Amemiya, Y. & Oya, M. (1995). *J. Phys. Chem.* **99**, 6652–6660.

Hirai, M., Niimura, N., Zama, M., Mita, K., Ichimura, S., Tokunaga, F. & Ishikawa, Y. (1988). *Biochemistry*, **27**, 7924–7931.

Israelachvili, J. N. (1992). *Intermolecular and Surface Forces*. London: Academic Press.

Israelachvili, J. N., Mitchell, D. J. & Ninham, B. W. (1976). *J. Chem. Soc. Faraday Trans. II*, **72**, 1525–1568.

Kawai-Hirai, R., Enomoto, A. & Nakamura, K. (1995). *Nippon Nogei Kagaku Kaishi*, **69**, 331–336.

Kawai-Hirai, R. & Hirai, M. (2003). *J. Appl. Cryst.* **36**, 489–493.

Kotlarczyk, M., Huang, J. S. & Chen, S. H. (1985). *J. Phys. Chem.* **89**, 4382–4386.

Leodidis, E. B. & Hatton, T. A. (1989). *Structure and Reactivity in Reversed Micelles*, edited by M. P. Pileni, pp. 270–302. Amsterdam: Elsevier.

Mazitov, R. K. (1981). *DAN*, **260**, 1402–1404.

Mitchell, D. J. & Ninham, B. W. (1981). *J. Chem. Soc. Faraday Trans. II*, **77**, 601–629.

Pal, S., Vishal, G., Gandhi, K. S. & Ayappa, K. G. (2005). *Langmuir*, **21**, 767–778.

Pileni, M. P. (1989). Editor. *Structure and Reactivity in Reversed Micelles*. Amsterdam: Elsevier.

Pitzalis, P., Angelico, R., Soderman, O. & Monduzzi, M. (2000). *Langmuir*, **16**, 442–450.

Uedaira, H. & Tataru, T. (1998). *Introduction to Molecular Physiology of Water*. Tokyo: Medical Science International, Ltd.

Ueki, T., Hiragi, Y., Kataoka, M., Inoko, Y., Amemiya, Y., Izumi, Y., Tagawa, H. & Muroga, Y. (1985). *Biophys. Chem.* **23**, 115–124.